Characterization and Fabrication of Functionally Graded Materials using Directed Energy Deposition

[1]Imran Bashir and [2]Aisha Kabir
[1,2]Begum Rokeya University, Modern Bypass, Rangpur 5404, Bangladesh.
[1]imranrokeyauniv@hotmail.com, [2]kabira5404@gmail.com

Correspondence should be addressed to Aisha Kabir : kabira5404@gmail.com

Article Info
Journal of Computational Intelligence in Materials Science (https://anapub.co.ke/journals/jcims/jcims.html)
Doi: https://doi.org/10.53759/832X/JCIMS202402008.
Received 10 January 2024; Revised from 06 March 2024; Accepted 12 April 2024.
Available online 06 May 2024.

Abstract – The purpose of this article is to use directed energy deposition (DED) to fabricate and test functionalized materials (FGMs). FGM is a horizontal zone exhibiting a smooth transformation from Ti-6Al-4V to Invar, with pure Invar at the highest level. Sophisticated techniques such as X-ray diffraction, scanning electron microscopy, microhardness testing, electron backscattering diffraction, transmission electron microscopy and energy dispersion chamber respectroscopy were employed to assess the microstructure, chemical composition, and mechanical features of FGM. This study highlights many advantages of FGM, such as increased thermal resistance, mechanical properties, thermal protection, scratch resistance, strong adhesive surfaces, related to analytical methods, material improvement and provide insights. The findings provide insights into the potential applications of FGM in many settings. Future research should prioritize the investigation of the mechanical properties of the FGM, paying particular attention to tests to determine their strength, flexibility, and stiffness.

Keywords – Additive Manufacturing, Calculation of Phase Diagrams, Scanning Electron Microscopy, Directed Energy Deposition, Functionally Graded Material.

I. INTRODUCTION

The qualities of a Functionally Graded Material (FGM) will exhibit a progressive shift depending on its location. The property gradient in the material arises from variations in chemical composition, microstructure, or atomic order that are depending on location. In the scenario where the chemical composition varies depending on location, the gradient may be determined using the transition function $c_i(x, y, z)$. This function depicts how the concentration of the component ci changes with respect to position. The practical value of functionally graded composites having a graded structure was acknowledged in theoretical publications by Udupa, Rao, and Gangadharan [1] as early as 1972. Nevertheless, the effectiveness of their efforts was constrained, perhaps attributable to a dearth of appropriate manufacturing techniques for FGMs at that period. It was not until 15 years later that systematic study on manufacturing procedures for functionally graded materials was conducted as part of a national research program on FGMs in Japan. Subsequently, a significant portion of the research on FGMs has focused on the processing of these materials, resulting in the development of a wide range of manufacturing techniques.

The manufacturing process of a FGM typically involves two main steps: constructing the spatially non-uniform structure (known as "gradation") and converting this structure into a solid material (referred to as "consolidation"). Gradation processes may be categorized into three types: constitutive, homogenizing, and separating processes. Constitutive procedures involve the gradual construction of a graded structure using precursor materials or powders. Recent advancements in automation technology have made it possible to implement constitutive gradation methods in a cost-effective manner. Homogenization processes involve gradual rotation of a distinct boundary between two objects by the movement of the objects. The separation process begins with a uniformly distributed substance, then transforms into a heterogeneous substance by the movement of particles by gravitational or electric fields from external forces. Processes of homogenization and fragmentation established continuous gradients, but they have limitations in introducing steep slopes of the species

Additive manufacturing (AM) has been proposed as the most efficient method for fabricating FGMs with favorable stress distribution and high formability. Furthermore, AM has been proposed as the most efficient method. This enables complex

processes that would be very difficult to reliably produce with conventional machinery. As a result, there are environmental advantages associated with this manufacturing process. Lu et al. [2] employed fused deposition modeling (FDM) to create samples with intricate geometric shapes, including as gyroid, cubic lattice, and Celtic knot patterns. In the following sections, we will provide a description and analysis of the many AM methods that have been created for the production of FGMs.

Nevertheless, AM plays a crucial role as a technique that allows for the step-by-step creation of metal FGMs with varying chemical compositions on a larger scale, often in the range of tens of millimeters. Directed Energy Deposition (DED) AM involves the direct introduction of powder or wire material into a pool of melting created by a source of heat. A laser is utilized to create a melt pool (MP) in the layer or substrate underneath when powder feedstock is being used. Powders are supplied into the melt pool by nozzles connected to several hoppers. DED may be used to fabricate FGMs by manipulating the proportions of two or fine particles introduced into the MP according on their location. Various FGMs with various component alloys have been investigated in the current body of research. These include Fe/FeAl, Ti-6Al 4V/ Inconel 718, TiAl, TiC/Ti, Ti-6Al-4V/γ- and Invar 36 (64 weight percent Fe, 36 weight percent Ni).

We used DED to create a FGM by combining AISI type 304L spotless steel with Inconel 625. The main purpose of this research is to assess the chemical compositions, microstructures, and microhardnesses of both the primary and secondary phases. The remaining sections of the research are arranged as follows: Section II discusses the aims and limitations of the research. Section III presents a critical analysis of previous literature works related to directed energy deposition system, fabrication process, and composition of FGM. In Section IV, a methodology employed to compose this article is presented. Section V presents a critical discussion of the results, defining the context of the study, computational analysis, and the manner in which the findings are presented. Lastly, Section VI draws a conclusion to the research, and recommends directions for future research.

II. RESEARCH OBJECTIVES AND LIMITATIONS

This work aims to analyze the mechanical properties, chemical composition, and microscopic structure of a directed energy deposition fabricated Functionally Graded Material (FGM). FGM is a horizontal area that exhibits a smooth transition from Ti-6Al-4V to Invar, with pure Invar in the uppermost part. This paper seeks to investigate the method of FGM and determines its stages including the changes that occur at each stage.

Various methods of characterization are used to accomplish these goals. EDS is used to analyze the chemical composition, while SEM is used to analyze the grain morphology. Microhardness is tested using a Vickers indenter to determine current phases, while XRD patterns are collected. TEM and EBSD are techniques for analyzing elemental structure and phases found on a microscopic scale. It is possible that the CALculation of PHAse Diagrams (CALPHAD) method provides better insight into the current phase of FGM and predicts structure reliable part of the equilibrium.

However, there are constraints to this research. Currently, there is no existing comprehensive thermodynamic database that encompasses the whole constituent variation to Invar from Ti-6Al-4V. Instead, a revised ternary Fe-Ni-Ti system components are used as an approximation. The validity of this estimate is due to the restricted occurrence of V and Al within the CR of the FGM. The limitations of the commercially accessible multi-element repository for this structure are also acknowledged.

III. RELATED WORKS

Directed energy deposition system

According to Ansari, Jabari, and Toyserkani [3], AM has been extensively reviewed, with a range of topics covered including dynamic process and post-processing. Dass and Moridi [4] primarily discuss a type of AM process called DED, also referred to as laser metal accumulation system, laser engineered net shaping (LENS™), directed laser deposition, and blown powder additive manufacturing. The print metals capacity and maybe any system of metal-alloy—especially functionally graded products—makes this technology remarkable. DED is also used for repairing or remanufacturing conditions in order to extend their lifetime and minimize their environmental effect.

DED systems, as covered by Mikulčić et al. [5], are made up of a continuous raw material flow and a highly concentrated energy source. These two components meet at a central location, often in the inert shield gas presence. Due to the intense power density in a specific location, the raw materials present there undergo melting, resulting in the formation of a pool of molten material. DED systems include many types such as wire-feed and powder-feed, which vary in the kind of feedstock used. Another type is melt-based DED, also known as melt-B DED. Additionally, there is kinetic energy-B DED, which varies depending on the specific energy source used. Several subtypes of melt-B directed energy deposition (DED) exist, such as electron-beam-B, electric arc-B, laser-B, and plasma-B.

The Powder-B Directed Energy Deposition (DED) methodology has been thoroughly examined in academic literature and is widely identified as the recommended approach for metal DED applications [6]. Typically, a laser beam serves as the primary heat source. Wired DED technologies exhibit lesser resolution than laser-beam powdered procedures, but provide a greater accumulation rate and the capability to construct bigger compositions. The heat source often used includes an electric arc, plasma, or electron-beam. Electron-beam based additive manufacturing (EBAM) [7] utilizes a concentration electron beam within a vacuum ecosystem to efficiently bond almost all types of metals. EBAM is commercially available via Sciaky, Inc. and is primarily employed for the production of near net form components. Plasma-based additive manufacturing employs a regulated plasma source to liquefy the metal particles. Norsk Titanium is using this recently developed additive manufacturing technique primarily for the production of titanium components.

In [8], the wire feed is melted using electric arc based DED to deposit the layers. The use of electric arc welding principles in metal Big Area Additive Manufacturing (mBAAM) enables the printing of large components. Kinetic energy dependent DED structures, often known as Cold Spray, use a nozzle with an intersecting-branching pattern to propel particles of micron size at supersonic speeds. When the impact velocity reaches a certain threshold, particles that are just a few microns in size stick to the surface and accumulate material, forming a coating or separate bulk components. This phenomenon has been seen and documented in [9]. **Fig 1** presents a flowchart that provides a concise overview of the many types of DEDS.

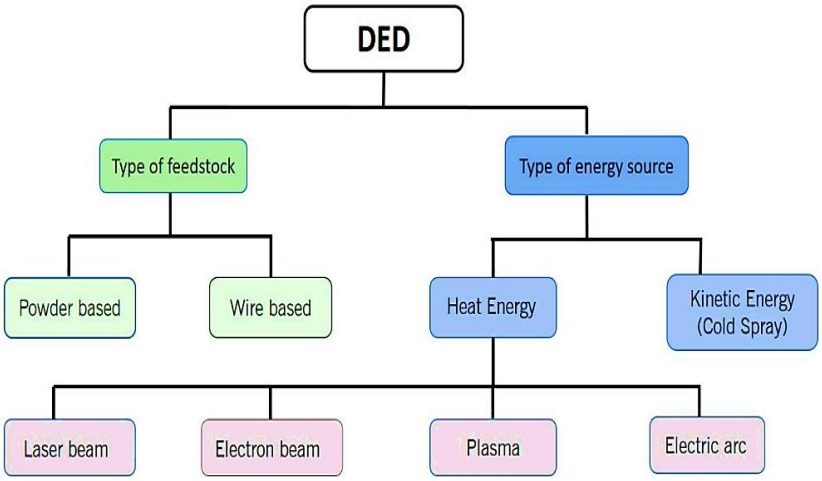

Fig 1. DED system classification

Fabrication process

Although the component was successfully produced without any visible fractures, Zhang et al. [10] determined, via both computational and experimental analysis, that a secondary phase consisting of transformation alloy carbides evolved in the gradient zone, resulting in the formation of micro-cracks. Su et al. [11] researched the phase compositions mechanical characteristics, and elemental composition, of two distinct FGMs: one that transitioned to pure V from Ti-6Al-4V, and another that transitioned to Invar 36from 304L pristine steel. The VFGM from Ti-6Al-4V displayed noticeable variations in composition, and stages along the slope.

In [12], several FGM samples developed cracks during the manufacturing process due to the production of brittle phases. The ultimate alloy Fe concentrations to Invar slope from 304L SS are equivalent. Even though the Coefficient of Thermal Expansion (CTE) reduced to 0.01 10-6 K-1 in Invar from about 15 10-6 K-1 in 304L SS, there was no fracturing in the slope zone of this FGM. About 10 mm into the slope area, something occurred. Garcin [13] successfully produced a ferromagnetic slope, with the Invar side exhibiting magnetic force characteristics and the paramagnetic capabilities exhibited by 304L SS. The authors hypothesized that multi-constituent phase diagrams may be used to enhance the performance of FGMs by preventing the formation of undesired phases, like brittle stages in the V FGM from Ti 6Al-4.

The square post samples in this study were created utilizing a directed energy deposition method. During the procedure, Ti-6Al-4V was layered with fine particles of Ti-6Al-4V in successive layers. Subsequently, there was an intermediate area where the quantity of Ti-6Al-4V was gradually reduced and substituted with pre-alloyed Invar powder. Finally, many layers of pure Invar were coated. Square posts were progressively refined, secured, and severe to effectively enhance examination. Mechanical elements, chemical composition, and microstructures of the samples were featured using approaches such as XRD, EDS, SEM, and micro-hardness testing. These samples indicated the availability of various stages such as hcp, bcc, C14, fcc, (Ni,Fe)Ti2 and DO24 phases.

Composition of the FGM

The concept of the structural gradient was founded in the early 1970s, as discussed in [14]. To mimic the properties and structure of natural products like teeth, bones, and bamboo trees. Functionally Graded Materials (FGM) were initially proposed for polymeric and composites products. The use of the notion of FGM was first introduced in Japan in 1984 during the space shuttle design phase. The aim was to produce the body using a material that has enhanced resistance to heat and increased mechanical qualities. This was achieved by progressively altering the compositions to ensure the body can endure a significant temperature differential of 1000 °C. **Fig 2** demonstrates the progression from pure metal to functionally graded metals. FGMs may serve as a thermal barrier and could be employed as a coating with good scratch resistance. FGMs, or functionally graded materials, may serve as a robust bonding interface to join two materials that are not compatible with one other.

Fig 3 depicts the potential variability of characteristics of traditional composites in comparison to FGMs. A single FGM is characterized by the presence of a scattered ingredient or phase that is not evenly distributed throughout the matrix, in contrast to typical composites. In double FGM, there are several constituents or phases present. A continuous slope is

achieved in all scenarios, contingent upon the density distribution of changes among the phases/constituents and the matrix being used.

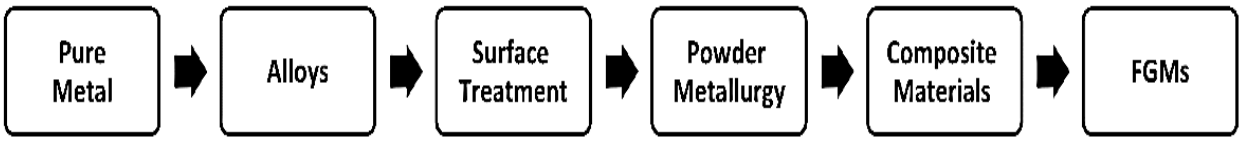

Fig 2. Progress in FGM-related materials

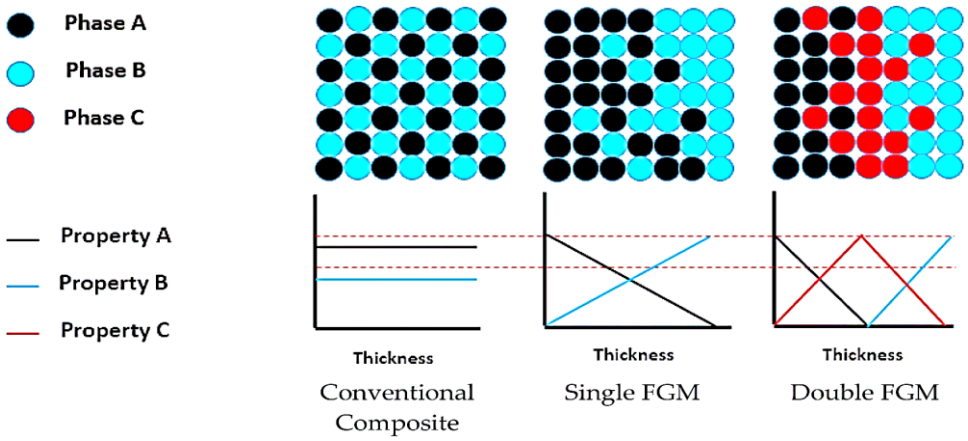

Fig 3. Differences in characteristics between traditional composites and FGMs

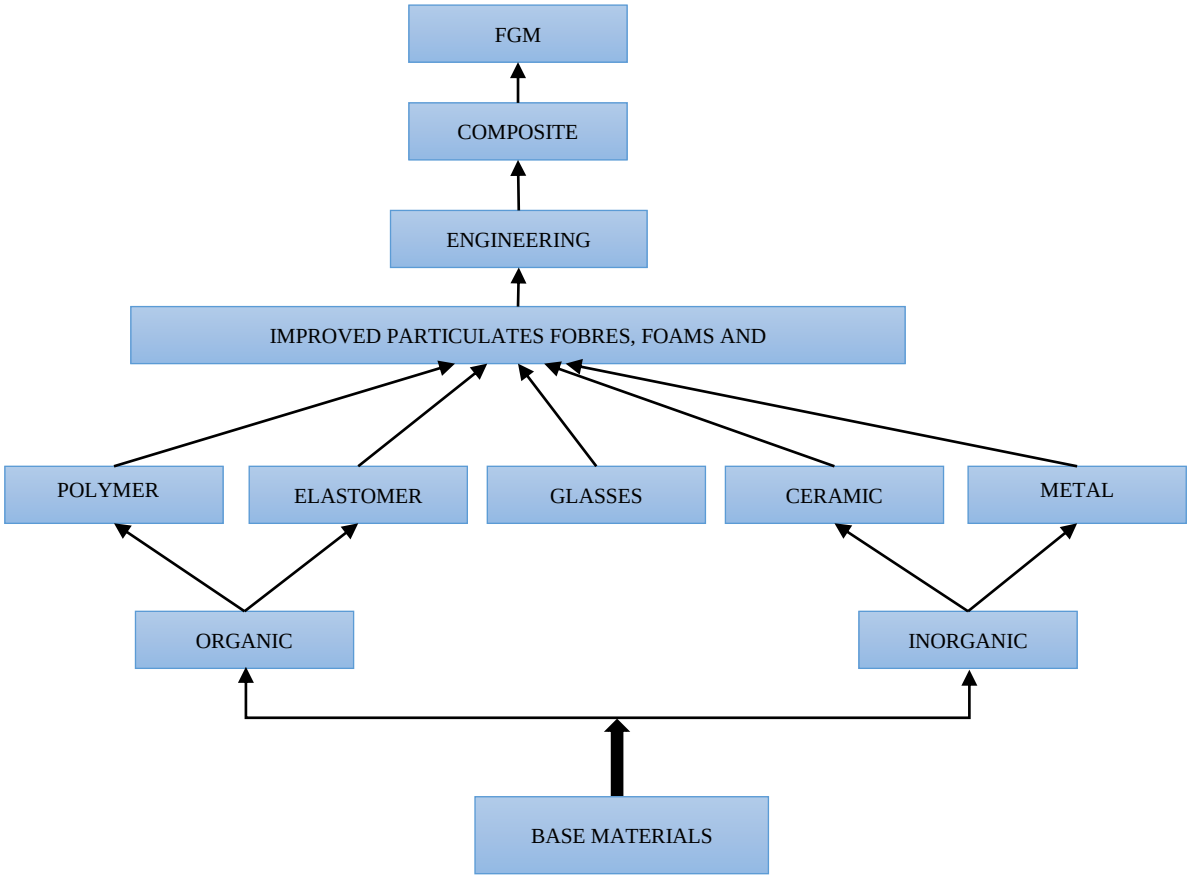

Fig 4. Visualization of contemporary material structure

According to Yılmaz et al. [15], Functionally graded materials, such as bones and teeth, are naturally occurring substances that have been engineered by nature to fulfill certain service needs. This concept is derived from nature in order to address engineering challenges, similar to how artificial neural networks are used to simulate the human brain. FGM

reduces the abrupt interfaces seen in composite material that is where issue is triggered. The abrupt contact is replaced by a gradient interface, resulting in a seamless transition between different materials. An exceptional attribute of FGM is its capacity to customize a material for a particular purpose.

According to Dobrzański and Dobrzańska-Danikiewicz [16], materials have been crucial in the development of our civilization and culture. The use of existing basic materials in scientific applications has paved the way for the improvement of new polymers, engineering alloys, structural ceramics, and other compounds. **Fig 4** depicts the developmental framework of contemporary materials. These materials have several characteristics that make them suitable for prospective applications. It encompasses the possibility of decreasing transverse stresses in both the in-plane and through-thickness directions, enhanced thermal characteristics, and high toughness, among other benefits.

IV. METHODOLOGY

This section outlines the methods used in generating the sample and examining its gradient properties. The specimen was created via a directed energy deposition technique, where Ti-6Al-4V fine particles 21 layers were added onto a Ti-6Al-4V base material. A slope zone was formed by systematically applying layers with a decrease of 3% in volume of Ti-6Al-4V and a matching increase of 3% in volume of Invar powder for each layer. The process was repeated for a total of 32 layers. Inver eventually added a total of 22 built-up floors. Later, the tree was cut, cut, placed, ground, and beautified for easy inspection.

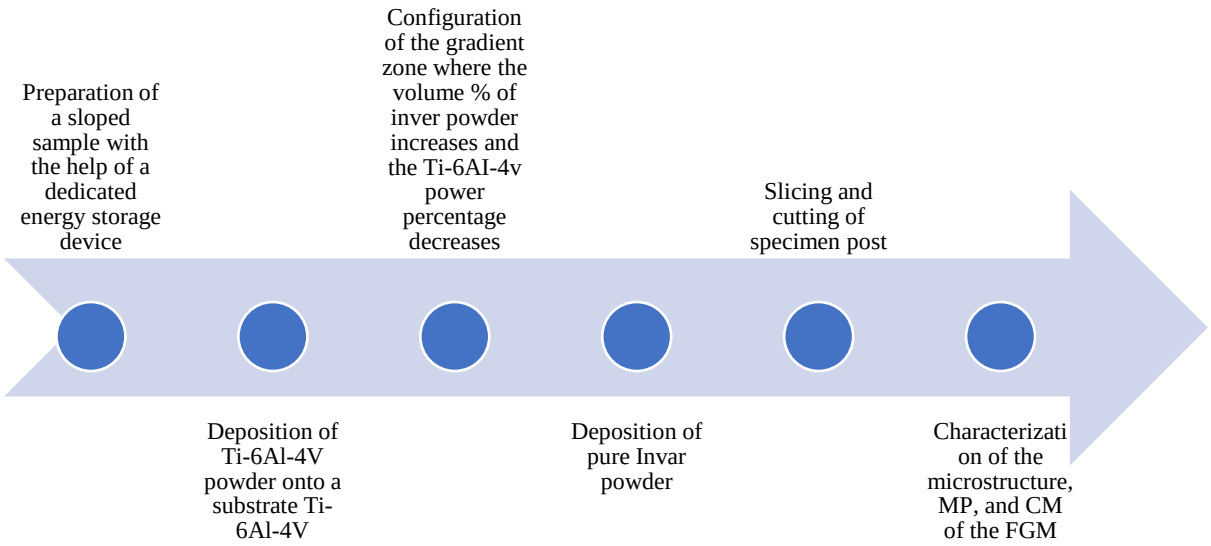

Fig 5. Progressive phases of the manufacturing process

The chemical composition, mechanical, and microstructure properties of FGM were investigated from different sources. In this study, we used scanning electron microscopy (SEM) [17] to investigate the morphology of the particles, and energy dispersive spectroscopy (EDS) [18] to investigate the elemental structure and spatial arrangement Using a Vickers intervention, the micro-hardness of the material was evaluated. The phases observed in the gradient area were recognized by X-ray diffraction (XRD) technique [19], the phases were further analyzed by electron backscatter diffraction (EBSD) [20] Thin foils were obtained using a focused ion beam microscale phase separation. Elemental species were then identified by examination of selected field diffraction patterns using transmission electron microscope (TEM) [21].

Furthermore, computational analysis used the CALPHAD method to accurately determine the combined equilibrium terms in the system. Since the current multicomponent databases are insufficient for this purpose, the sections in the central region of the FGM phase were identified by the Fe-Ni-Ti ternary system. Through a comprehensive analysis, we determined the temperatures at which the solid and liquid phases coexist. Additionally, the CALPHAD model accurately anticipated the presence of four additional phases. This article offers an elaborate account of the methodology used in the research's creation and the methodologies used for assessment, guaranteeing a precise and thorough study of the gradient sample. **Fig 5** provides a concise overview of the sequential stages involved in delineating the manufacturing process.

V. RESULTS AND DISCUSSION

Context of the study

304L unstained steel FGM, which was formed from a Ti-6Al-4V using DED throughout the manufacturing process, experienced cracking. Reichardt et al. [22] discovered that the introduction of stainless steel into the construct resulted in the

formation of Fe-V-Cr sigma and brittle FeTi phases, which subsequently caused cracking. Based on their findings and the Fe-V-Cr phase schematic obtained by Wang, Wang, and Sun [23], Niewolak et al. [24] suggested alternative gradient pathways that might prevent the production of sigma phase.

The current study included the fabrication of a sample utilizing DED, which was graded to Invar 36 from Ti-6Al-4V. The selection of these two terminal alloys was based on their distinct thermal and mechanical qualities. Invar exhibits an extremely low CTE of around 0.01 × 10-6 K-1 at ambient atmosphere. This characteristic makes it valuable for use in environments with significant temperature fluctuations, as it helps prevent thermal shock and ensures dimensional accuracy. Examples of applications that benefit from Invar's properties include telescope technology and the production of superior quality, accurate optical mirror substrates. In contrast, Ti-6Al-4V has a significantly greater coefficient of thermal expansion (CTE) at room temperature, measuring 8.5-10 × 10-6 K-1. Ti-6Al-4V, however, has a great power to the mass ratio of 246 kN-m/kg, a low density of 4.43 g/cm3, and corrosion resistance. In contrast, Invar has a high density of 8.05 g/cm3 and a correlatively lower power to mass ratio of 76 kN-m/kg. When these two alloys are straight in line bonded by different welding, intermetallic may form, which may create a weak spot or lead to failure.

Specifically, the huge disparity in CTE between the two alloys may lead to failure when exposed to substantial temperature variations, since the junction would serve as a site of stress concentration. Nevertheless, because to the ability of a FGM to achieve a progressive alteration in the elemental composition, the characteristics, such as the CTE, are expected to vary gradually across the gradient. This, in turn, reduces the probability of component failure when exposed to temperature fluctuations. Hence, the Ti-6Al-4V to Invar FGM exhibits promising prospects for use in very challenging environmental circumstances, such as those seen in nuclear or aerospace reactors. Examining this specific FGM (Functionally Graded Material) system may provide understanding on how computational forecasts and experimental analysis can be used to ascertain the feasibility of achieving a successful linear gradient route in grading two well recognized alloys. If not, it will provide understanding as to whether a different, non-linear method is required, and can be devised, via which this FGM may be effectively manufactured.

This study deviates from previous literature by employing an investigational-computational approach to both predict and measure the stages that form during the fiction of FGMs. The objective is to design the most effective slope pathway for this product system. The current study experimentally examined the phase composition, local microstructure, and elemental composition of the FGM at different positions. These characteristics were then compared to the properties and structure of the component alloys. Simulating the phase formations during FGM fabrication is very demanding because of the intricate temperature and AM processes composition profiles. Nevertheless, as shown by Yang et al. [25] and in our current study, well-chosen phase equilibrium computations may provide crucial insights for forecasting the strength of phases developed in FGM components.

Computation analysis

The slope sample was produced with a directed energy accumulation technique known as the RPM 557 Laser accumulation technique. The square post specimens were created by using a YAG laser with an energy output of 900W and velocity of 12.7 mm/s. These samples have a base area of 15 mm x 15 mm. The hatch angle was set at 90 degrees, indicating that the scanning direction rotated by 90 degrees for each layer. The vertical distance between each layer was 0.38 mm, while the horizontal breadth of each hatch was 0.58 mm. The manufacturing procedure was carried out under an argon environment.

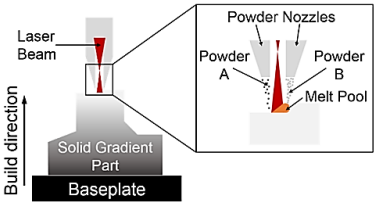

Fig 6. Images of the FGM material sorted from Invar to Ti-6Al-4V

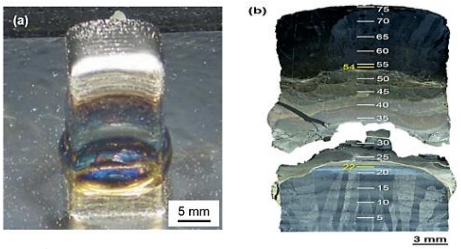

Fig 7. Contrast of Invar and Ti-6Al-4V images of FGM samples

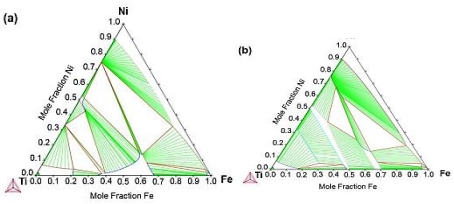

Fig 8. Phase equilibria determined by applying the Fe-Ni-Ti structural assessment at 1100K and the TCFE8 database

The accumulation system has the capability to apply up to four distinct powders throughout the manufacturing process, and permits the modification of the calibrated proportion of these fine particles by about 1% for each layer deposited. A Ti-6Al-4V stratum was covered in a total of 21 coatings of pre-alloyed (PA) Ti-6Al-4V fine particles using the Fused Granular Manufacturing (FGM) technique (see **Fig 6**). The next step was to deposit layers in a gradient region. For each layer, the capacity Ti-6Al 4V percentage was lowered by 3% in volume, and in its place, 3% in volume of PA Invar small particles were used. The moderate transformation to Invar from Ti-6Al-4V was finally entirely completed at coating 53 after 32 coatings of this procedure. Ultimately, a total of 22 layers composed entirely of Invar were applied, namely including coatings 54 to 75. The post reached a height of roughly 28.5 mm.

During the process of removing the post from the baseplate and dividing it in half using the sample fractured vertically, wire electric dismissal machining, as seen in **Fig 7a**. Standard metallographic procedures were used to mount, grind, and polish the two halves of the material. Eight minutes was used for dispersion of 0.05 µm silica during the last polish. After that, for four seconds, the specimen was inscribed using Kroll's reagent, which is a solution of 3% nitric acid in water and 2% hydrofluoric acid. The mechanical characteristics, chemical makeup, and microstructure of the FGM were studied in relation to its geographical location. An SEM FEI Quanta 200 was used for the purpose of studying grain morphology. In addition to the SEM, an EDS system equipped with a (Oxford X-act PentaFET Precision) silicon drift detector was used to analyze the chemical composition and elemental segregation.

A V indenter (Leco V-100-C1) was used to measure the sample's microhardness during the course of the FGM. A 15-second dwell time and a 300 g load were applied. To determine the stages of the slope zone, X-ray diffraction (XRD) designs were obtained using a Panalytical Empyrean Bragg-Brentano-type diffractometer. The diffractometer comprised a copper K-alpha X-ray source, which functioned at a current of 40 milliamperes and a voltage of 45 kilovolts (corresponding to a wavelength of 1.54 angstroms). To do further stage investigations, we also employed EBSD, Oxford Nordlys Max2. The small-scale phase analysis was accomplished by using Quanta 200 3D Dual Beam FIB to remove thin foils from a single layer of the bulk material. To conduct small-scale elemental composition investigation and get specified region diffraction patterns, (FEI Talos F200X, TEM, and FEI Technai G2 20 XTWIN) was used.

The balance stage relations of the structure were predicted using the CALPHAD approach in order to assist in determining secondary phases along the slope. Although AM is a procedure that occurs outside of equilibrium, it involves the faster molten material solidification and subsequent thermal cycles. By conducting phase calculation of equilibrium at various atmospheres and covering the entire range of chemical composition, valuable information can be obtained about the present phases in the FGM, as shown by Yan et al. [26]. The primary concern is to choose a temperature that is in close proximity to the point at which the desired phase changes begin to undergo kinetic freezing. A comprehensive thermodynamic database that encompasses the complete constituent variation to Invar 36 from Ti 6Al-4V is not currently accessible. This is due to the fact that multi-component thermodynamic databases are typically tailored to specific alloy systems, like TTI3 for alloys of titanium from ThermoCalc, PanTitanium for alloys of titanium from CompuTherm, and the TCFE8 database for steels.

In order to overcome the limitations of current databases with several components, the ternary Fe-Ni-Ti subsystem [27], which has been newly redesigned, was used to identify the stages inside the central region of the FGM post. This estimate is considered plausible due to the relatively hypotonic of aluminum (Al) and vanadium (V) in the FGM post configuration variation. Utilizing the modified ternary Fe-Ni-Ti subsystem lessens some of the issues with the existing trading multi-element repository for this system, as seen in **Fig 8**. More precisely, there are variations in stage balance, particularly at 1100 K, between the Fe-Ni-Ti system evaluation conducted recently and that estimated using the TCFE8 database. The most current phase diagram indicates constant solid solvability from FeTi to B2 NiTi; however, this phase is lacking on the Fe-Ti side of the ternary measure section anticipated using the TCFE8 repository, likely due to the repositories` lack of coverage in the high Ti content area. Expanding into the region is the C14 Laves phase.

Presentation of findings

Fig 7b illustrates that at around layer 26 of the FGM, there is evidence of layers overflowing the layers underneath. **Fig 9** provides the liquids and solidus conditions determined for the slope zone spanning from pure Ti to Invar. These computation shows that the liquidus and solidus bends decrease by about 650 K when the capacity percentage of Invar is roughly 0.1-0.2, corresponding to coatings 25-29. The CALPHAD framework was used to ascertain the secondary stages that formed throughout the manufacturing process, based on their location within the gradient. **Fig 10** depicts the equilibrium phase diagram at a temperature of 1100 K, which accurately forecasts the emergence of four further phases. The temperature was chosen because it is lower than both the beta trans us and the solidus curve.

The phases were forecasted to form at balance: NiTi2 (unclassified structure), FeTi (B2), Ni3Ti (DO24), and Fe2Ti (C14, Laves). It is important to acknowledge that all compounds exhibit a high degree of solubility for the third element that is dissolved within them. The classification used in this context are just for the purpose of convenience in distinguishing between distinct phases. In addition, the ordered B2 phase and the bcc phase are represented by a single Gibbs power function, indicating that they are considered as a single phase. The phase diagram in equilibrium revealed the existence of thefcc Invar and bcc titanium main phases, together with a tiny area of hexagonal close-packed (hcp) titanium near the titanium corner.

The phases in this paper are named as: hcp (solution of solid) of Ti, Ni, and Fe with a higher concentration of Ti), B2/bcc (a Ti-rich SS of Ti, Ni, and Fe with both disorder and an arranged surrounding according to NiTi, and FeTi, with Fe, Ni, and Ti having specific ranges of composition), C14 (according to Fe2Ti with specific varies of Ti, Fe, and Ni composition), fcc (according to the Invar alloy with specific variations of Fe, Ni, and Ti composition), DO24 (according to Ni3Ti with specific variations of Ti, NI, and Fe composition), (Ni,Fe)Ti2 (according to NiTi2 with specific variations of Ti, Ni, and Fe composition). There is interchangeability between these phase identifications.

At 1100K, the hcp solution stage gives way to the bcc solution phase, moving to Fe-36Ni from pure Ti. The bcc stage remains in an area with just one phase until the volume fraction of Invar reaches 12%. At this point, the formation of NiTi2 starts. At about 24 volume percent, the body-centered cubic (bcc) structure of Invar ceases to exist, resulting in the presence

of solely NiTi2 with dissolved Fe. Subsequently, the formation of B2 is initiated, leading to the complete disappearance of NiTi2 at a concentration of 36 volume.% Invar. A Laves stage C14 starts to replace B2 when the Invar alloy reaches a volume fraction of around 42%. The B2 phase completely disappears when the Invar alloy reaches a volume fraction of 55%. Subsequently, when the Invar alloy reaches around 82% volume percent, both Ni3Ti and C14 phases completely disappear, leaving just the face-centered cubic (fcc) phase. Shortly thereafter, a small quantity of Ni3Ti starts to form.

Fig 9. Solid and liquid temperatures in relation to the constituent along the vertical axis ranging from pure Titanium to Invar (an alloy consisting of 36% Nickel and Iron). With a rise in the mass fraction of Invar, both the solidus and liquidus atmospheres see a significant decrease of around 700 K. The temperatures reach their lowest points, around 1300 K, when the Invar content is at 12% and 18% in volume.

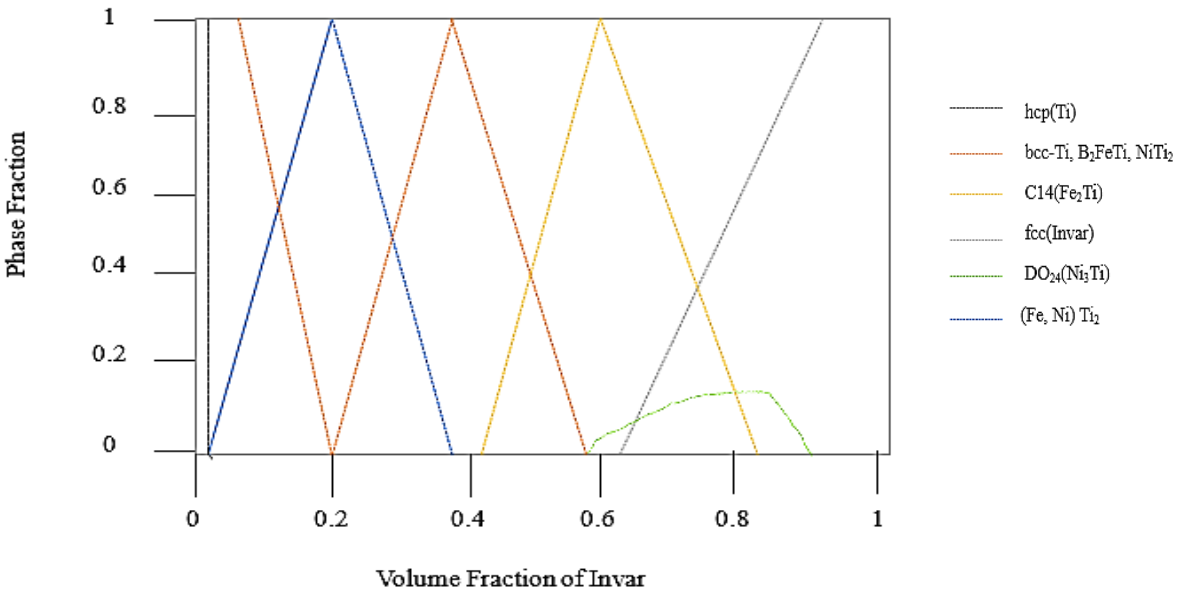

Fig 10. Molar phase fractions, as projected by CALPHAD frame-working, at 1100 K in VS to Invar from pure Ti, as a composition function.

The work used a directed energy deposition technique to fabricate a sample with a gradient structure. The sample consists of alternating layers of small particles of Invar and Ti-6Al-4V. Over time, the volume percentage of Invar increases. Then, the samples were prepared for testing by cutting, forming and polishing procedures. Different methods were employed to

group the mechanical properties, chemical composition, and sample microstructure, such as SEM, microhardness testing, EDS and sample analysis using X-ray diffraction. Determining various phases was determined by the assessment of many samples such as XRD, and ENSD. Predicting was executed using the CALPHAD technique, and the results showed the availability of various stages ((Ni,Fe)Ti2, DO24, hexagonal close-packed (hcp), face-centered cubic (fcc), C14, and body-centered cubic (bcc), which different amount according to their invar percentages.

VI. CONCLUSION

In this paper, a discussion of specimen preparation using direct energy deposition (DED) has been presented. This method integrates pure Invar, Invar series, and powdered Ti-6A1-4V. Various experimentations were done to effectively categorize the chemical composition, mechanical and micro-structural features of the materials. In the experimentation, various techniques (electron backscatter diffraction, scanning electron microscopy, and X-ray diffraction) were utilized to effectively characterized the depression zone. The findings of the experiments indicated the presence of various techniques on the gradient, such as (Ni,Fe)Ti2, DO24, fcc, C14, bcc/B2, and hcp. Future research should focus on the mechanical features of the molded materials samples. All these materials use tensile, fatigue, and compression tests to evaluate material strength, ductility, and durability. Additionally, advanced microscopy techniques such as transmission electron microscopy provide detailed examination of phase microstructure and distribution. Other computational models can be used to increase the understanding of phase changes during fabrication and the accuracy of phase prediction.

Data Availability

No data was used to support this study.

Conflicts of Interests

The author(s) declare(s) that they have no conflicts of interest.

Funding

No funding was received to assist with the preparation of this manuscript.

Competing Interests

There are no competing interests.

References

[1]. G. Udupa, S. Rao, and K. V. Gangadharan, “Functionally Graded Composite Materials: An overview,” Procedia Materials Science, vol. 5, pp. 1291–1299, Jan. 2014, doi: 10.1016/j.mspro.2014.07.442.

[2]. R. Lu, S. Chandrasekaran, W. L. Du Frane, R. L. Landingham, M. A. Worsley, and J. D. Kuntz, “Complex shaped boron carbides from negative additive manufacturing,” Materials & Design, vol. 148, pp. 8–16, Jun. 2018, doi: 10.1016/j.matdes.2018.03.026.

[3]. M. Ansari, E. Jabari, and E. Toyserkani, “Opportunities and challenges in additive manufacturing of functionally graded metallic materials via powder-fed laser directed energy deposition: A review,” Journal of Materials Processing Technology, vol. 294, p. 117117, Aug. 2021, doi: 10.1016/j.jmatprotec.2021.117117.

[4]. A. Dass and A. Moridi, “State of the art in directed energy deposition: from additive manufacturing to materials design,” Coatings, vol. 9, no. 7, p. 418, Jun. 2019, doi: 10.3390/coatings9070418.

[5]. H. Mikulčić, J. J. Klemeš, M. Vujanović, K. Urbaniec, and N. Duić, “Reducing greenhouse gasses emissions by fostering the deployment of alternative raw materials and energy sources in the cleaner cement manufacturing process,” Journal of Cleaner Production, vol. 136, pp. 119–132, Nov. 2016, doi: 10.1016/j.jclepro.2016.04.145.

[6]. S. Liu and Y. C. Shin, “Additive manufacturing of Ti6Al4V alloy: A review,” Materials & Design, vol. 164, p. 107552, Feb. 2019, doi: 10.1016/j.matdes.2018.107552.

[7]. S. Negi et al., “Review on electron beam based additive manufacturing,” Rapid Prototyping Journal, vol. 26, no. 3, pp. 485–498, Nov. 2019, doi: 10.1108/rpj-07-2019-0182.

[8]. T. Abe, D. Mori, K. Sonoya, M. Nakamura, and H. Sasahara, “Control of the chemical composition distribution in deposited metal by wire and arc-based additive manufacturing,” Precision Engineering, vol. 55, pp. 231–239, Jan. 2019, doi: 10.1016/j.precisioneng.2018.09.010.

[9]. C. M. Greer et al., “Introduction to the design rules for Metal Big Area Additive Manufacturing,” Additive Manufacturing, vol. 27, pp. 159–166, May 2019, doi: 10.1016/j.addma.2019.02.016.

[10]. C. Zhang et al., “Additive manufacturing of functionally graded materials: A review,” Materials Science and Engineering: A, vol. 764, p. 138209, Sep. 2019, doi: 10.1016/j.msea.2019.138209.

[11]. Y. Su, B. Chen, C. Tan, X. Song, and J. Feng, “Influence of composition gradient variation on the microstructure and mechanical properties of 316 L/Inconel718 functionally graded material fabricated by laser additive manufacturing,” Journal of Materials Processing Technology, vol. 283, p. 116702, Sep. 2020, doi: 10.1016/j.jmatprotec.2020.116702.

[12]. S. Farahmand, A. H. Monazzah, and M. H. Soorgee, “The fabrication of Al2O3–Al FGM by SPS under different sintering temperatures: Microstructural evaluation and bending behavior,” Ceramics International, vol. 45, no. 17, pp. 22775–22782, Dec. 2019, doi: 10.1016/j.ceramint.2019.07.318.

[13]. T. Garcin, “Thermodynamic and kinetic effects of static magnetic field on phase transformations in low-alloy steels,” 2009. [Online]. Available: https://tel.archives-ouvertes.fr/tel-00519996

[14]. K. P. Able and B. R. Noon, “Avian community structure along elevational gradients in the northeastern United States,” Oecologia, vol. 26, no. 3, pp. 275–294, Jan. 1976, doi: 10.1007/bf00345296.

[15]. E. Yılmaz, F. Kabataş, A. Gökçe, and F. Fındık, “Production and characterization of a Bone-Like porous TI/Ti-Hydroxyapatite functionally graded material,” Journal of Materials Engineering and Performance, vol. 29, no. 10, pp. 6455–6467, Oct. 2020, doi: 10.1007/s11665-020-05165-2.

[16]. L. A. Dobrzański and A. Dobrzańska-Danikiewicz, "Why are Carbon-Based materials important in civilization progress and especially in the industry 4.0 stage of the industrial revolution," Materials Performance and Characterization, vol. 8, no. 3, p. 20190145, Aug. 2019, doi: 10.1520/mpc20190145.
[17]. F. Orsini et al., "In situ Scanning Electron Microscopy (SEM) observation of interfaces within plastic lithium batteries," Journal of Power Sources, vol. 76, no. 1, pp. 19–29, Nov. 1998, doi: 10.1016/s0378-7753(98)00128-1.
[18]. I. M. Saleh, I. E. Ruyter, M. Haapasalo, and D. Ørstavik, "Adhesion of endodontic sealers: scanning electron microscopy and energy dispersive spectroscopy," Journal of Endodontics, vol. 29, no. 9, pp. 595–601, Sep. 2003, doi: 10.1097/00004770-200309000-00013.
[19]. B. D. Cullity, Elements of X-ray diffraction. 1956. [Online]. Available: http://cds.cern.ch/record/821266
[20]. F. J. Humphreys, "Characterisation of fine-scale microstructures by electron backscatter diffraction (EBSD)," Scripta Materialia, vol. 51, no. 8, pp. 771–776, Oct. 2004, doi: 10.1016/j.scriptamat.2004.05.016.
[21]. S. Kook et al., "Automated Detection of Primary Particles from Transmission Electron Microscope (TEM) Images of Soot Aggregates in Diesel Engine Environments," SAE International Journal of Engines, vol. 9, no. 1, pp. 279–296, Sep. 2015, doi: 10.4271/2015-01-1991.
[22]. A. Reichardt et al., "Development and characterization of Ti-6Al-4V to 304L stainless steel gradient components fabricated with laser deposition additive manufacturing," Materials & Design, vol. 104, pp. 404–413, Aug. 2016, doi: 10.1016/j.matdes.2016.05.016.
[23]. W. Wang, W. Wang, and Q. Sun, "Influence of Microstructure on Corrosion Properties of Fe–V Alloy from Vanadium Slag," Metals and Materials International, Sep. 2023, doi: 10.1007/s12540-023-01523-6.
[24]. L. Niewolak, L. Garcia-Fresnillo, G. H. Meier, and W. J. Quadakkers, "Sigma-phase formation in high chromium ferritic steels at 650°C," Journal of Alloys and Compounds, vol. 638, pp. 405–418, Jul. 2015, doi: 10.1016/j.jallcom.2015.03.076.
[25]. L. Yang, Y. Wang, X. Wu, and J. Shi, "Nonequilibrium thermodynamic calculation and experimental investigation of an additively manufactured functionally graded material," Journal of Alloys and Compounds, vol. 838, p. 155322, Oct. 2020, doi: 10.1016/j.jallcom.2020.155322.
[26]. L. Yan et al., "A review on functionally graded materials and structures via additive manufacturing: from Multi-Scale design to versatile functional properties," Advanced Materials Technologies, vol. 5, no. 6, Apr. 2020, doi: 10.1002/admt.201900981.
[27]. L. D. Bobbio et al., "Design of an additively manufactured functionally graded material of 316 stainless steel and Ti-6Al-4V with Ni-20Cr, Cr, and V intermediate compositions," Additive Manufacturing, vol. 51, p. 102649, Mar. 2022, doi: 10.1016/j.addma.2022.102649.